Printing Anisotropic Appearance with Magnetic Flakes

THIAGO PEREIRA, Princeton University
CAROLINA L. A. PAES LEME, Universidade Federal do Rio de Janeiro
STEVE MARSCHNER, Cornell University
SZYMON RUSINKIEWICZ, Princeton University

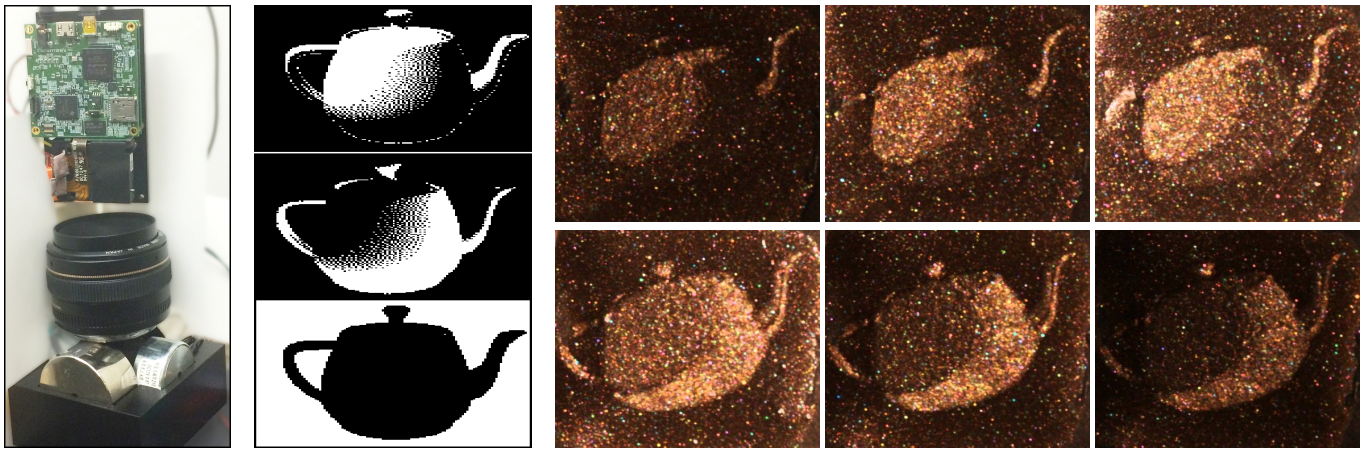

Printing setup Spatial patterns Printed result under varying lighting

Fig. 1. *Left:* Our setup consists of a DLP projector modified to project UV light, a focusing lens, and five electromagnets surrounding a target (not visible) coated with magnetic flakes in a UV-curable resin. *Center:* We use the electromagnets to orient the flakes in three configurations, then solidify the resin in particular spatial patterns. *Right:* Observing the surface under different illumination directions, we see that it exhibits spatially-varying reflectance.

The ability to fabricate surfaces with fine control over bidirectional reflectance (BRDF) is a long-standing goal in appearance research, with applications in product design and manufacturing. We propose a technique that embeds magnetic flakes in a photo-cured resin, allowing the orientation distribution of those flakes to be controlled at printing time using a magnetic field. We show that time-varying magnetic fields allow us to control off-specular lobe direction, anisotropy, and lobe width, while using multiple spatial masks displayed by a UV projector allows for spatial variation. We demonstrate optical effects including bump maps: flat surfaces with spatially-varying specular lobe direction.

CCS Concepts: • **Computing methodologies** → **Reflectance modeling**;

Additional Key Words and Phrases: Fabrication, Spatially-Varying BRDF

ACM Reference format:
Thiago Pereira, Carolina L. A. Paes Leme, Steve Marschner, and Szymon Rusinkiewicz. 2017. Printing Anisotropic Appearance with Magnetic Flakes. *ACM Trans. Graph.* 36, 4, Article 123 (July 2017), 10 pages.
https://doi.org/10.1145/3072959.3073701

1 INTRODUCTION

There has been considerable recent progress on digital fabrication of objects, providing for fine control over geometry and appearance. A long-term goal is to provide designers with the ultimate in flexibility: being able to create an object with arbitrary shape, where the reflectance at each point can be set to an arbitrary physically-realizable bidirectional reflectance distribution function (BRDF). While there has been recent progress towards this goal, existing methods are limited in the reflectance they can reproduce. They are usually restricted to isotropic reflectance [Matusik et al. 2009; Dong et al. 2010; Hašan et al. 2010; Papas et al. 2013] or simple patterns of anisotropy [Lan et al. 2013; Levin et al. 2013; Ye et al. 2014].

In this work we aim to broaden the set of BRDFs that may be fabricated using inexpensive and practical means. We use inks with reflective magnetic flakes, whose orientation distribution may be controlled by applying an external magnetic field [Pratt and Salzberg 1947]. These particles are embedded in a carrier liquid that lets them rotate, but is also UV-curable. We can therefore selectively fix the flakes in place, allowing us to create a surface with spatially-varying flake orientations, hence spatially varying BRDF.

Our approach is inspired by micro-facet BRDF models [Cook and Torrance 1982; Ashikmin et al. 2000], in which the major features of the BRDF come from the distribution of facet orientations in a small surface element. Instead of facets on a surface, we print using

flakes inside a thin volume and control their orientation distribution with the magnetic field. Even though in this paper we are restricted to 2D printing, these flakes could also be used when printing volumes. This would enable a direct physical implementation of the micro-flake model [Jakob et al. 2010], allowing for fabrication of subsurface scattering effects.

Although this paper presents an early prototype, using magnetic flakes for svBRDF printing has a number of advantages. First, it can achieve high spatial resolution, unlike early work that explicitly fabricated "macroscopic" facets [Weyrich et al. 2009]. It can also produce surfaces that exhibit specular reflection with an effective local surface normal that differs from the global normal — in other words, bump maps — as well as anisotropic reflectance with spatially-varying tangent maps. Our technique is inexpensive and compatible with 3D printing, since it uses essentially the same stereo-lithography technology to achieve spatial variation; the only additional hardware is a few electromagnets.

Section 3 describes our selection of magnetic flakes, binder medium, and final ink composition. We present a qualitative discussion of the behavior of the flakes under magnetic fields, which motivates our setup (Section 4) that incorporates electromagnets and a UV projector. We describe how to control the printed BRDFs, using *time-varying* magnetic fields (Section 5) to achieve effects such as control over specular direction and lobe width, as well as anisotropy. Finally, Section 6 shows our measurements of these BRDFs and Section 7 shows some spatially varying results.

2 RELATED WORK

Magnetic flakes: Using a magnetic field to orient reflective particles in ink was first proposed by Pratt and Salzberg [1947]. The authors use a rotating magnetic field created by solenoids to align reflective flakes horizontally, making the ink more specular. More recent applications of these flakes have involved orienting them with more complex *static* magnetic fields. This produces appearance that changes with light/view direction, effectively producing specular surfaces with varying local normals (Figure 2). The technique has found applications in security printing [Kashiwagi et al. 1994; Benninger et al. 2005]. For example, bank notes may include some characters with magnetically oriented flakes. Matching the reflectance of these characters is impossible with standard isotropic printer flakes and is still hard without access to the exact magnetic field that created it. Magnetic flakes have also been used in the cosmetics industry, such as in magnetic nail polish [Thevenet 2008]. After a coating is applied to a nail, a custom-shaped magnet is applied and quickly creates spatial variation of reflectance. For this application, the spatial variation is the major aspect, although the result is a light/view dependent appearance.

Different mechanisms for creating images by orienting magnetic particles have been proposed in the literature, using custom shaped magnets by either cutting [Kashiwagi et al. 1994] or milling [Benninger et al. 2005]. Their main limitation is that the magnetic field does not change with time, which limits the range and reproducibility of the achieved BRDFs. In addition, the resulting orientation field is continuous and no hard edges can be created (Figure 6). One approach to create spatially-varying results with edges is UV-curing, and the use of multiple static magnetic fields coupled with multiple masks to selectively block UV light has been proposed [Phillips et al. 2004]. Kokkinis et al. [2015] use UV curing with magnetic particles oriented using dynamic (rotating) magnetic fields, and combine spatial variation in magnetic flakes with 3D printing.

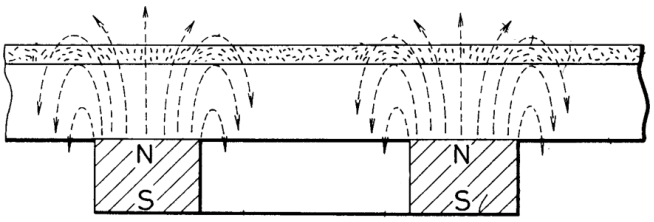

Fig. 2. A spatially varying magnetic field (dashed lines) created by two magnets is used to orient reflective particles (top layer). Image from [Kashiwagi et al. 1994].

Our work is inspired by the above techniques, but we aim at moving from qualitative control over BRDF to producing *specific* BRDFs, at high spatial resolution. We use a computer-controlled electromagnet and UV projector to achieve both a wider range of spatially-varying effects and, more importantly, more *predictable* results. We adopt a computational fabrication methodology, in which we characterize the capabilities of our fabrication device and then optimize for how to drive the device to achieve a result as close as possible to a target appearance.

Appearance fabrication: There has been considerable work on using computer-controlled fabrication in novel ways to affect a surface's appearance; see the state-of-the-art report by Hullin et al. [2013] for a recent summary. Two important classes of methods for goal-based BRDF fabrication are those that use scattering flakes and those that use continuous surfaces.

Papas et al. [2013] fabricate objects of a uniform material that achieves a prescribed subsurface light diffusion profile (BSSRDF) using a mixture of isotropic scattering pigments in a transparent medium. Other approaches [Dong et al. 2010; Hašan et al. 2010] use a 3D printer to fabricate a spatial arrangement of isotropic scattering materials that approximates a spatially-varying BSSRDF. All these works are focused on the spatial dimension of the BSSRDF and ignore its angular dimension. Matusik et al. [2009] uses a dithered combination of glossy and diffuse inks to reproduce a target spatially-varying reflectance function. Due to the use of glossy inks, their approach allows for controlling specular reflection. However, all these works restrict themselves to unoriented flakes. In our work, we use oriented flakes to achieve anisotropic results. This is made possible by our use of a magnetic field to orient particles.

Surface based approaches [Weyrich et al. 2009; Finckh et al. 2010; Papas et al. 2011] are more flexible in creating anisotropic reflectance (e.g., even teapot-shaped highlights can be achieved) but must use all available resolution to control angular reflection. As a consequence, no spatial variation is achieved. This is largely a consequence of surface continuity, which restricts their methods to smooth surfaces, causing an effective loss in resolution. Two recent works use light diffraction to achieve high spatial resolution, but with limitations on angular control. The work of Levin et al. [2013]

is limited to symmetric specular peaks, and does not allow for non-symmetric reflectance such as off-specular peaks. Ye et al. [2014] can produce off-specular peaks, but with only a small bending angle away from the specular direction, and at high cost. Our setup, in contrast, allows for significant off-specular reflection and builds on inexpensive 3D printing technology.

Finally, a recent approach takes a hybrid road. Lan et al. [2013], in a two step process, use a 3D printer to create anisotropic bumps and print glossy inks over them. Even if their inks are isotropic, they can achieve anisotropic results with the underlying geometry. Our method can create anisotropic reflectance using only paper and ink, with no 3D object necessary. For cases in which a 3D object is desired, their approach could be used together with our oriented flakes. This would extend the range of manufacturable appearance in their method even further.

3 FLAKES AND COMPOSITION

Metallic and pearlescent paints achieve their characteristic appearance by incorporating flakes (small facets) that reflect light. Some of these, developed for applications such as security printing and cosmetics, are magnetic. This allows for the construction of a printing system in which the flake orientation distribution, and hence scattering, can be externally controlled. These flakes are usually composed of a flat substrate of mica, coated with layers of magnetic iron oxides and titanium dioxides [Raksha et al. 2007]. Color is produced via interference, and is controlled by varying layer thickness.

Choice of flakes: We use magnetic flakes available commercially from Colorbridge. We tested flakes in two size distributions: 5–25 microns and 10–60 microns. Both have a glittery appearance, but it is less pronounced with the smaller flakes. On the other hand, we were able to orient the larger flakes more consistently, leading to the ability to produce narrower BRDF lobes. We therefore choose to use the larger flakes in this work.

Choice of medium: Our application requires a medium that at first allows the flakes to move, and then hardens to fix them in place. This may be achieved with either evaporative solvents or UV-curable resins. Magnetic flakes embedded in a solvent are readily commercially available as "magnetic nail polish" [Thevenet 2008], which is distributed with a special magnet that produces a spatially-varying field. The polish is intended to be used by applying it to the nail, bringing the magnet close to the nail, and waiting for the polish to dry (Figure 3). However, it is difficult to achieve controlled orientation and spatial variation with a solvent-based medium.

A UV-curable medium has a number of advantages for printing BRDFs. First, the resin hardens only when desired. Flakes can be exposed to magnetic fields for as long as needed, as opposed to solvents that lock the flakes in place in a few seconds. Second, these resins allow us to *selectively* harden pixels: we exploit this to create spatially varying BRDFs by printing in multiple passes.

Although UV-curable nail polish containing magnetic flakes is commercially available, its visual quality is low, perhaps due to low concentration or low quality of flakes. We therefore mix raw magnetic flakes, as described above, with clear UV gel nail polish. We have also experimented with 3D printer resin, which works similarly to the gel but may present a greater toxicity hazard.

Fig. 3. Commercially available magnetic nail polish is used to create reflective patterns on nails. A magnet is brought close to the nail, reorienting the flakes and thus creating spatial variation. This pattern is fixed in place when the nail polish dries.

Concentration: We performed an experiment to compare the BRDFs of different concentrations of flakes in the UV-curable gel. In this example, we used compositions at 1%, 6%, 12%, 18%, and 30%, where the concentration is measured in mass of pigment divided by total mass of composition. These five samples have the same thickness, since the composition is applied between two glass slides placed a fixed distance apart.

Figure 4 shows specular reflections produced by inks with these five concentrations, after orienting the flakes with a bar magnet. The lowest concentration of 1% shows a weak highlight meaning that, as expected, the ink is largely transparent. As concentration increases past 12%, we see that the lobe width increases, so that we can no longer align the flakes as consistently: they begin to physically interfere and can no longer be oriented parallel to each other, given the strength of this magnetic field. (Stronger magnetic fields can yield better alignment, and hence narrower specular peaks.)

Because our final setup uses an electromagnet to orient the flakes, and uses fields that are weaker than the bar magnet used for this initial experiment, we chose to use the 6% concentration. This does not require strong fields and achieves good alignment even with our electromagnets. If we had a stronger setup, we would expect a composition around 12% to be a better choice, since in that case varying field strength could be used to achieve an even wider range of BRDF lobe widths.

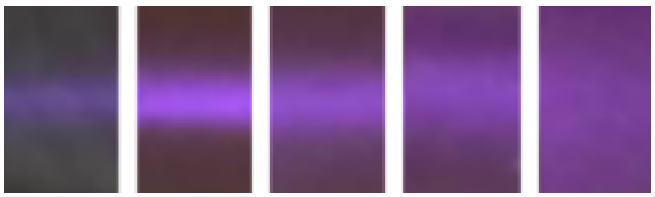

Fig. 4. *Left to Right:* Increasing pigment concentration in a UV-curable composition. The color variation in each sample is caused by a static spatially varying field. The normals of the flakes at the center of each image are pointing towards the viewer, while the normals at the top and bottom are increasingly tilted away from the viewer.

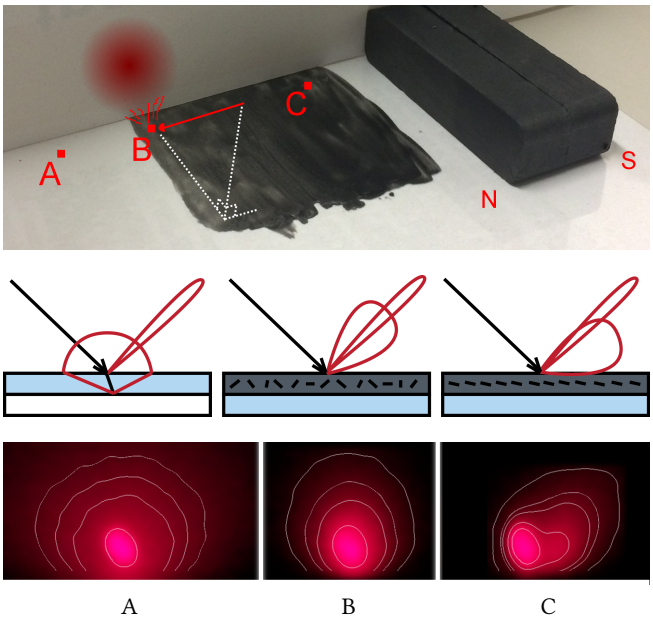

Fig. 5. *Top:* Experimental setup in which a laser illuminates three different points. Point A (left) is a transparency on top of white paper shown here only for comparison. Point B (center) is unoriented ink. Point C (right) is oriented ink. *Middle:* Depictions of the three points' reflective lobes. The light that exits each point hits a vertical white sheet of paper. *Bottom:* The images formed on paper, with iso-contours of intensity. By orienting the flakes in the ink, we can create an off-specular lobe in a controllable direction (right).

Our final mixture also incorporates 10% isopropyl alcohol by mass into the composition. Even this small percentage lowers the viscosity, which also makes it easier for the flakes to align. Higher concentrations of alcohol, unfortunately, interfere with curing.

3.1 Magnetic Alignment

In this section, we introduce a qualitative discussion of the appearance of magnetic flakes in static magnetic fields. We discuss experiments using magnetic nail polish, but the results are essentially the same with the UV-curable composition. In section 6, we quantitatively support these conclusions with BRDF measurements of these flakes. These static field results are already used in security printing and cosmetics. We show them here only to provide more intuition on the appearance of these particles in a spatial arrangement. We first look at BRDFs at specific points, then we look at spatially varying BRDFs created with static magnets.

In a first experiment, we used a bar magnet to orient flakes applied on a transparency (Figure 5). This experiment shows how the BRDF depends on the direction of the magnetic field. For this setup, the painted surface is mostly near the north pole of the magnet. While we are not depicting the magnetic field lines, their effect is to tilt the flakes' normals towards the magnet. They tilt by some amount at the point labeled C and are mostly unaffected at the point B due to the distance to the magnet. We use a laser with an elevation angle of roughly 45 degree to shine light in the selected points. The light distribution exiting each point hits a vertical sheet of paper of which we take a photo. We show both diagrams and pictures of the reflectance of each point. First, we show a transparency sheet overlaid on white paper (point A). Its resulting reflectance is composed of mirror reflection at the air-transparency interface plus a diffuse lobe given by the paper. The diffuse lobe is shown as a reference BRDF. It is interesting to notice that points A, B and C all show similar specular reflection lobes, produced by either the air-transparency or the air-ink interface. When the paint is present there is no wide diffuse lobe; instead, the light that goes into the ink is reflected by the flakes. For point B (center), this creates a much smaller glossy lobe surrounding the mirror reflection. Finally point C has oriented flakes, which create an off-specular lobe in a position that can be controlled by orienting the flakes. When images are created using these flakes, it is this off-specular lobe that we are mainly concerned with, since most view directions are not aligned with the ideal specular direction. Nevertheless, all samples in this work still have a specular reflection from their top surface.

Fig. 6. A spatially varying magnetic field can be used to create spatially varying reflectance. *Left:* Horseshoe-shaped magnets were placed 3 mm below a sheet of paper. *Right:* A coating of nail polish was applied to the paper, giving the impression of a bump map. We remind the reader that this sample is completely flat.

We can also place the magnet underneath (or above) the paper. Results produced using this method are shown on the nail in Figure 3 and also in Figure 6, where we placed two arc shaped magnets 3 mm below the paper while applying the nail polish. Once again, the paint is completely flat. In both figures, the result resembles a bump map with a specular material, providing strong motivation for our technique.

4 PRINTING SETUP

In this section, we describe our setup for printing of spatially-varying BRDFs (Figure 1, left). The main idea is to use the UV-curable composition and a sequence of projected patterns with UV light. We apply a dynamic magnetic field to change the flake orientation distribution, and hence the BRDF, and then harden only a subset of pixels with the projector. This process locks the flakes at those locations, while others are still free to move. For example, to print a checkerboard with two BRDFs, we would apply the first magnetic field and then illuminate the white squares in the checkerboard, completing the first pass. Then we would apply the second magnetic field and illuminate the black squares of the checkerboard, completing the second pass.

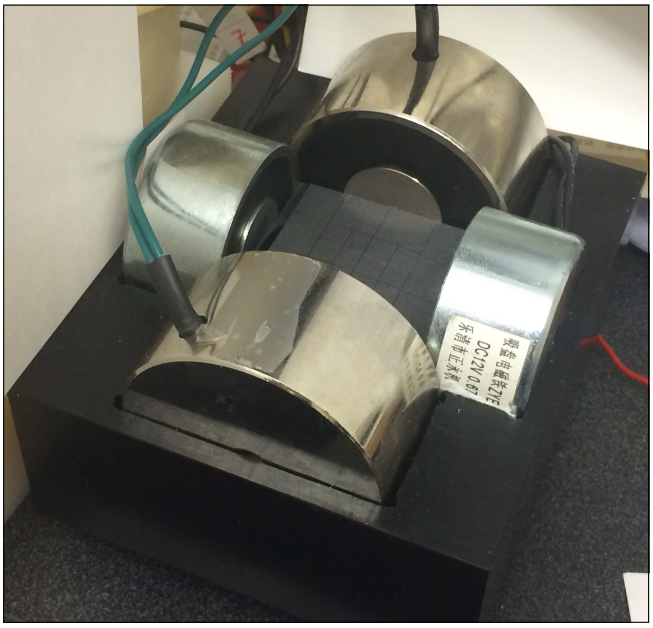

Fig. 7. Our magnetic setup includes 5 electromagnets in a custom-milled holder. Two pairs achieve a relatively uniform field in the x and y axes, while only a single z magnet below the sample (not shown) is used to leave one side open for the projector.

4.1 Magnetic Setup

Our system requires us to produce a uniform and controllable magnetic field, which we accomplish with a set of electromagnets (Figure 7). While our solution provides 3-DoF control over the field, fast switching, strong intensity, low cost, and easy integration with a projector, this comes at the cost of limited spatial range of approximately 1×1 cm.

We use a total of 5 electromagnets: 2 each for the x and y axes, and a single magnet for the vertical z direction. This is necessary to leave one side of the setup open for the projector. We position the magnets as closely together as possible, to maximize field intensity. Indeed, even though the far-field falloff of a magnet is $1/r^3$, by operating in the near-field regime we observe intensity falloff closer to $1/r^{2.5}$. The x and y magnets are located approximately 2 cm from the center of the printing region, while the z magnet is closer — about 1.6 cm — to compensate for the fact that it acts alone and not part of a pair.

The electromagnets are driven with an Arduino microcontroller with current augmented using an external 24 V power supply. PWM control, smoothed by an RC filter, allows for precise control over currents, up to 700 mA per electromagnet.

Calibration: One undesirable consequence of only using one magnet for the z axis is that it produces diverging magnetic field lines, leading to lower uniformity than in the x and y axes. Our solution to this problem is to use the other four magnets to compensate for the non-uniformity of z. At a high level, this works by running both x magnets (same for y) with opposite currents, such that they cancel each other at the exact center but still create a non-zero field

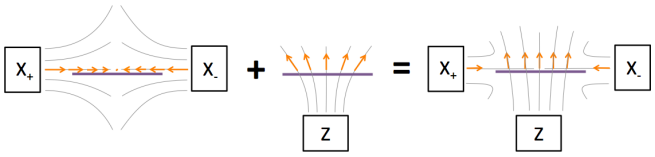

Fig. 8. The pairs of x and y magnets are used to increase field uniformity. They partially cancel the opening of the field created by the z magnet. We show a diagram for the x magnet.

around the center that can be used to cancel deviations from the z magnet (Figure 8).

In order to implement this, we need to find the current to run through each magnet. We measured the responses of all five magnets at multiple locations on the printing plane. All measurements were performed by moving a magnetic sensor with two linear stages. The response of each magnet was measured multiple times with different input currents, and we used the slope of the resulting line, which is more robust to noise and background magnetic field.

We then solve for the five currents necessary to produce a target magnetic field, averaged across multiple x, y positions. Optimizing for multiple positions creates a more spatially uniform field. This process can be written as a linear system. Since scaling all the currents scales the magnetic field, we only solve the linear system for target fields on a unit hemisphere. The other side of the sphere can be found by simply scaling all currents by -1.

All of this happens as a pre-computation. In order to have these results accessible by the microcontroller code, we gather the five currents calculated by the linear system and fit a fourth degree polynomial in two dimensions u, v. We chose u, v to be a stereographic mapping of the hemisphere, since it introduces lower distortion.

Using the original measurements of each magnet and the optimized currents, we can simulate the field combinations and calculate the average (over all possible fields and positions) angle between the desired field and the achieved field. We calculated this angle error to have a mean of 3.4 and a maximum of 5.1 degrees. To validate this process, we re-measured the field for 5 different magnetic field targets at 4 different locations in the printing plane in an 8×8 mm square. Over this smaller set of 20 measurements, we observed a mean error of 2.5 and max of 7.3 degrees. These numbers contrast with the much larger errors if we do not use 5 magnets simultaneously: the naive solution of driving x, y, and z independently gives a mean measured error of 5.8 degrees and maximum error of 18 degrees.

Our final system can achieve fields of 9000 μT. (For reference, this is about 200 times the earth's magnetic field.) We had to scale down all currents uniformly in order to have the maximum current calculated with the linear system be the maximum current delivered by the system. This uniform scaling results in a roughly 40% loss in total intensity. This loss could be reduced by using constrained optimization.

4.2 Projector Setup

The other component of our setup is a projector along the z axis. We use the DLP Lightcrafter from Texas Instruments, with one of its color LEDs replaced with a high-power 385nm UV LED (model

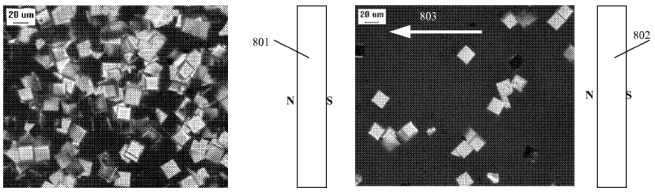

Fig. 9. Microscopic images of magnetic flakes, taken from [Raksha et al. 2009]. *Left:* Initially, flakes have random orientations. *Right:* After applying a magnetic field (created by a pair of magnets oriented as shown), the facets align with their diagonal directions along the magnetic field, i. e. left to right. Note that the image at right shows a lower concentration of flakes.

number LZ110UA00-U4 by LED ENGIN). We power this LED with a current of 800 mA. Since our magnetic field is only uniform in a small area, it is necessary to project an image in a small area as well, and we use an SLR lens in reverse to focus the projector onto the target.

During our printing process, we project each image for 20 seconds. This is enough to partially cure the resin and stop the flakes from realigning with new fields. At the same time, this is short enough to mostly limit "leaking" to adjacent pixels that are black and should not be cured. (See discussion of leakage in Section 7.) At the end of the printing process, we project a full white frame and cure all pixels for an additional 30 seconds.

The curing time of 20 seconds per frame compares to the 45 seconds it takes to align the flakes for each projected image. This means that curing is not the bottleneck in our printing process. In our experiments with stronger magnetic fields (produced with bar magnets), we find that it is possible to bring this alignment time to a few seconds, which would make curing the bottleneck and suggest the use of a stronger LED.

5 CONTROLLING BRDFS WITH MAGNETIC FIELDS

This section describes our experiments with time-varying magnetic field schedules (shown in Figure 10) and our observations of the BRDFs they generate. The qualitative results discussed here are supported by measurements in the next section.

Our strategy for controlling BRDF with magnetic fields is motivated by the observations of Raksha et al. [2009], who have taken microscopic images of flakes before and after application of a magnetic field (Figure 9). This image shows that most of the flakes align along their diagonals, and also that the alignment is good but not perfect. Looking more closely, we see that one diagonal of each flake aligns with the magnetic field, but the flakes are also free to rotate around the x axis. This implies that a constant magnetic field causes greater light spread in one direction (the y axis) than in the other (the x axis). We will refer to this as the "extra" degree of freedom when aligning magnetic flakes in a static magnetic field.

This extra degree of freedom presents an opportunity, since it enables us to achieve anisotropic reflectance distributions; but it also presents a challenge, because the process of aligning flakes with a static field will lead to different results depending on the starting configuration of flakes. We can think of the alignment process as being state dependent. This has two practical consequences: sensitivity to initial randomness and dependence on history.

First, whenever the composition with flakes is deposited, the flakes will have some random initial orientation distribution (see qualitative depiction in Figure 11, left). This orientation is usually not completely random, and in fact it depends on how the composition was applied. For example, applying these flakes with a brush already causes some anisotropy aligned with the brushing direction. Whatever the deposition method, a system that aims at good repeatability of BRDFs needs to "clean" this initial non-randomness of the flakes. In fact, in a printing process with multiple passes such as ours, this cleaning process needs to be applied repeatedly to remove the effects of previous passes as well.

Second, the dependence on magnetic field history means that we have much more flexibility: different *sequences* of magnetic fields will be useful, as long as each sequence generates a different, repeatable, BRDF. If history did not matter, then the only degrees of freedom at our disposal would be field intensity and direction, which would limit the range of achievable BRDFs. We now describe some time-varying magnetic field schedules that we have experimented with and the BRDFs they generate. Experimenting with other schedules could lead to interesting future work.

5.1 Circular Field

In the earliest work with alignment of magnetic flakes, Pratt and Salzberg [1947] showed one way to control the extra degree of freedom. They used two electromagnets, creating two horizontal magnetic fields in the x and y directions. By simply switching each field on and off in sequence, they obtained good alignment of the facets' normal directions along the z axis (Figure 11, second column), resulting in a specular sample.

Since our setup has x, y, z control and also supports digitally-controlled continuous current levels (instead of just on and off), we use a natural extension of their alternating field: an arbitrarily tilted circular field (Figure 10, left). Given a normal direction n and two vectors (u, v) spanning the plane perpendicular to n, the field is

$$B_{circ}(t) = B_0\,(u\cos\omega t + v\sin\omega t), \tag{1}$$

where B_0 is the intensity of the field and $\omega = 2\pi f$, with a frequency f of 2 Hz.

As in Pratt and Salzberg's experiment, this also leads to improved alignment of the flake distribution, but lets us control the lobe direction (Figure 11, third column). The parameter B_0, as well as the total time for which the field is applied, can be used to control the degree of alignment, and hence the specular lobe width, assuming random initial flake orientations.

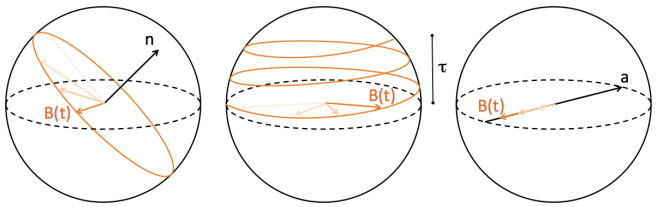

Fig. 10. Time varying magnetic fields used to orient flakes. The flake distributions resulting from these fields are shown in Figure 11.

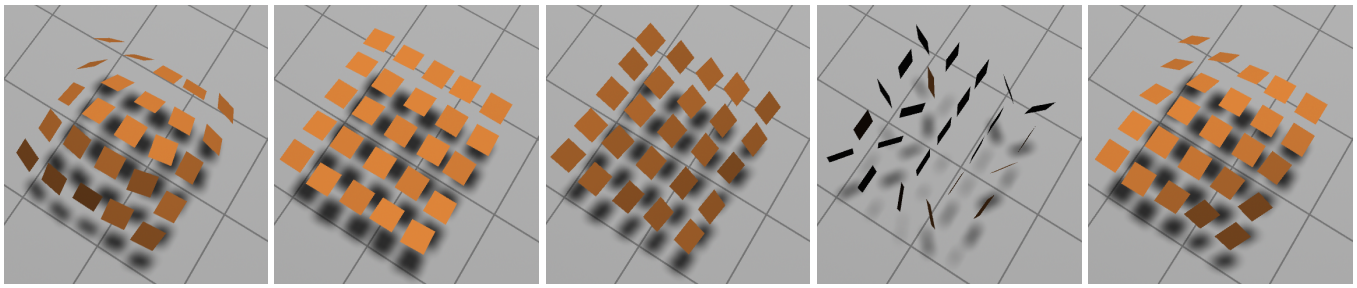

Unoriented / spiral | Circular pointing up | Circular tilted right | Spiral to vertical | Line

Fig. 11. Qualitative depictions of flake orientation distributions resulting from applying different time-varying fields. The resulting BRDFs would be, from left to right, mildly specular, highly specular, highly specular with a tilted peak, dark (approximately diffuse), and anisotropic.

5.2 Random Field

In order to achieve spatially-varying BRDFs with different orientations and lobe widths, we need the ability to reset the flake orientation to be random or close to random. An intuitive first attempt at a cleaning process would be to apply a sequence of *random* fields (varying at, say, 2 Hz). We found that while this sequence was able to clean initial deposition marks, it had an undesirable side effect. It usually introduced some tilt in the flake distribution. In other words, the peak of the BRDF lobe was not in the direction of the normal, but instead got stuck in some other direction that we found difficult to control. Instead, we adopted a spiral field for cleaning.

5.3 Spiral Field

For both cleaning and producing specular peaks with wider-than-minimum lobe width, we found a spiral field (Figure 10, center) to be satisfactory. This starts as a circular field, but then the z component slowly increases to some maximum value τ, while keeping the field magnitude normalized. Increasing τ increases the lobe width, which also makes the appearance darker. This happens because many flakes try to align with the input field (which has a positive z component) and lose their alignment with the sample's normal (Figure 11, fourth column).

More specifically, we interpolate between a circular field and a constant vertical field $B_{vert} = (0, 0, 1)$:

$$B_{spiral}(t) = \frac{f(t)\, B_{circ}(t) + \Big(1 - f(t)\Big)\, B_{vert}}{\Big\| f(t)\, B_{circ}(t) + \Big(1 - f(t)\Big)\, B_{vert} \Big\|}, \tag{2}$$

where $f(t)$ controls the speed of interpolation. We use a thresholded Gaussian function $f(t) = \max[g(t), 1 - \tau]$, meaning that the interpolation starts out slow and stops when the z component has a value of τ.

This field does not suffer from the drawbacks of the random field, and generates lobes still centered in the direction of the sample's normal. It works as a consistent cleaning process to erase effects from previous fields and bring the flakes to a known distribution.

We have not experimented with more general spirals that start from an arbitrary plane spanned by u, v and move towards a normal direction n, but we expect it to work just the same.

5.4 Line Field

The last field we discuss is the line field (Figure 10, right), which we use to create anisotropic BRDFs. This field takes as input a tangent vector a in the x-y plane, and oscillates in the direction of this vector:

$$B_{line}(t) = a \sin \omega t. \tag{3}$$

If this field is applied right after the circular field, nothing happens. This is because all flakes are already planar and no longer exhibit the "extra" degree of freedom. Instead, we apply this field after the spiral. As such, the lobe width first grows with the spiral, and then the line field orients the flakes but still leaves the extra degree of freedom (Figure 11, right). In this way, the final result is anisotropic.

5.5 Frequency of Fields

As described above, our circular oscillations happen at 2 Hz. We found that a substantially slower oscillation speed, e.g. 0.5 Hz, resulted in too much influence from recent field directions, while too high a frequency, e.g. 10 Hz, resulted in slow convergence and even temporal aliasing phenomena. All of these speeds are dependent on material: we found that lower-viscosity nail polish required higher speeds by a factor of 2 or 3.

6 MEASUREMENTS

We have measured the BRDFs of magnetic flakes oriented using three of the dynamic magnetic field schedules: circular field, spiral field and line field. These measurements quantitatively show how BRDF parameters such as lobe width, direction, and anisotropy vary as a function of parameters of the magnetic schedules such as direction and intensity.

We used a gonioreflectometer to measure these BRDFs. During acquisition, the camera was fixed in the z direction with the light free to move on a hemisphere. This gives us a 2D slice of the BRDF, which is enough to characterize the major features of our flake distributions. The angle between the light and the camera varies between $-75°$ and $75°$ in increments of $5°$; the three samples at $-5°$, $0°$, and $5°$ are not acquired because the light source blocks the camera view direction. The highlight from the sample's surface is in this direction, but this is not a problem since we are most interested in measuring the off-specular lobe caused by the flakes.

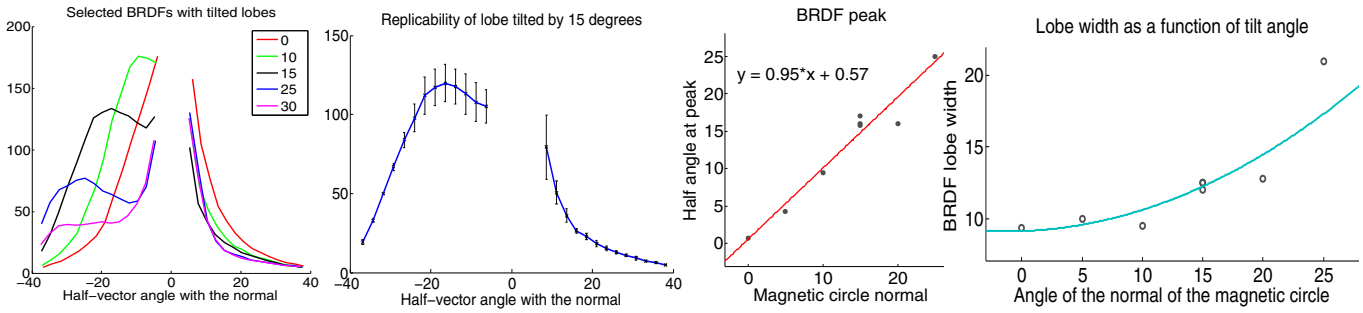

Fig. 12. (a) Normal-plane slice of reflectance measurements for samples with flakes tilted at $\alpha = 0, 10, 15, 25, 30$, plotted against half-angle. This shows the surface's specular highlight centered at 0 and also the off-specular peaks centered at increasing angles. (b) The $\alpha = 15^\circ$ sample repeated 3 times shows good repeatability of our orientation process. (c) We fit a parametric model to interpret how the off-specular lobe's peak and width changes with tilt angle. The center of the lobe is exactly the circular field's normal. (d) Lobe width increases when orienting at higher angles.

6.1 Circular Field

We measured the BRDF generated by circular fields to create flake normal distributions where the average normal makes some angle α with the painted sample's normal. Figure 12a shows reflectance measurements in the normal plane, for samples with $\alpha = 0^\circ, 10^\circ, 15^\circ, 25^\circ$, and 30°. The horizontal axis of this plot is the "half-angle" — the angle between the surface normal and the vector halfway between the light and view directions — which is the most relevant quantity when examining specular reflection. The plot shows the surface's specular highlight centered at 0 and also the off-specular peaks centered at increasing angles.

To explore the repeatability of our orientation process, we measured three different samples at $\alpha = 15^\circ$. Figure 12b shows the mean BRDF as a solid line, together with the corresponding error bars. In our setup, we do not have a mechanism to control the thickness of the samples, and the inks are initially applied by hand. We believe that this is the main source of variation.

In order to interpret our data, we fit a parametric model to slices of the off-specular lobes with center, width and amplitude as free parameters. For low α values such as 0 and 5, a simple Laplacian distribution ($A\exp(-|x-u|/b)$) fits the data well. In log space this is an absolute value function where A is the amplitude, u is the center and b is the lobe width (or deviation). However, for higher α values the off-specular peaks tend to be more round. We add a single additional radius parameter that controls a transition from Gaussian to Laplacian near the peak, which results in good fits to the rounded peaks. With increasing α, we obtain a tilted peak center, as expected. Figure 12c shows how the half-angle of the center of the lobe follows the flake tilt direction α. The lobe width also increases with α (Figure 12d), while the amplitude decreases.

We also oriented the samples using a series of horizontal circular fields with increasing intensity. All these BRDFs are centered (lobes at 0 degrees), but they show variation in the specular lobe. Figure 13, left, shows how the lobe width decreases with increasing field strength. At intensity 0, we can see the lobe width of unoriented flakes is around 13 degrees. It decreases to around 9.5 at high intensity. Figure 13, right, also shows how the amplitude increases. We expect the lobe width to decrease further with stronger fields.

6.2 Spiral Field

We next investigate the spiral field. As described in the previous section, this field takes a parameter of the maximum z component to which it converges. As this parameter is increased, the lobes get wider and darker, as shown in Figure 14, left and right. An interesting feature of both these transitions is that they happen suddenly, with a transition threshold around 0.3.

6.3 Line Field

We demonstrate anisotropic BRDFs generated with the line magnetic field. Figure 15 shows five hand-painted samples with tangents of, from top to bottom, 0, 45, 90, 135, and 180 degrees. The samples are lit at constant elevation angle and with azimuthal angles varying from left to right: 0, 45, 90, and 135 degrees.

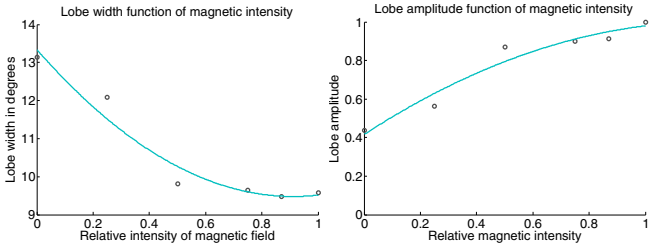

Fig. 13. Effect of magnetic field strength on the BRDF. As field strength increases, the lobe width decreases (left) while amplitude increases (right).

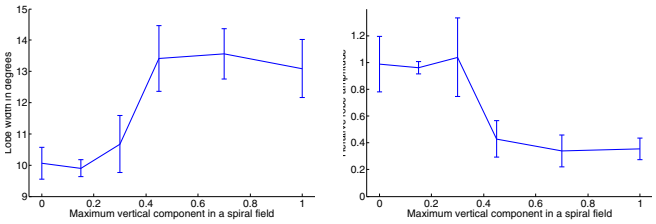

Fig. 14. By varying the maximum z component in the spiral field we can control lobe amplitude and width.

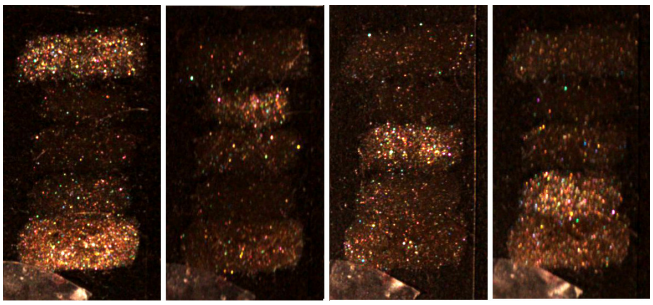

0° 45° 90° 135°

Fig. 15. Five anisotropic BRDFs with tangents of 0, 45, 90, 135, and 180 degrees (top to bottom). They are lit an elevation angle of 45° and four different azimuthal angles, as shown.

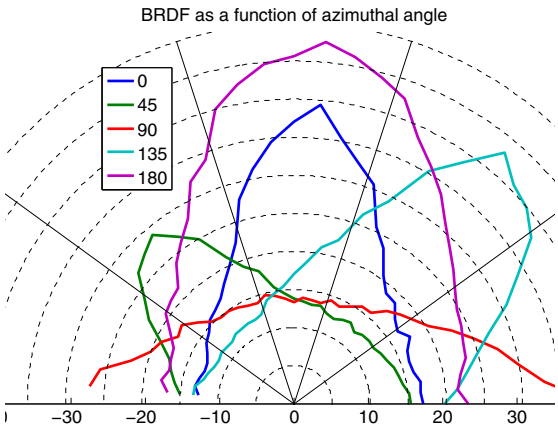

Fig. 16. Polar plot of anisotropic BRDFs oriented in different tangent directions by the line field. Each BRDF is shown as a function of light azimuthal angle, and is observed at an elevation of 45°.

Figure 16 shows slices of the measured BRDFs in a polar plot at a fixed elevation angle of 45 degrees. The major axis of each BRDF clearly aligns with the magnetic field direction. We observed a mean ratio between major and minor axis of 2.5 for these five samples in the plot. The ratio ranged between 2.3 and 2.9.

7 PRINTED RESULTS

In this section, we show BRDF prints using different magnetic field schedules. First, a SIGGRAPH logo (Figure 17) illustrates two different masks, where the logo has a specular BRDF and the background is made darker with the spiral field ($\tau = 1$).

Figure 1 shows a teapot printed with three different masks. The background used the spiral field, while two foreground masks were oriented with circular fields tilted towards the top and bottom of the image. We used dithering between the masks in this result to create a smoother transition. Unfortunately, we found that during the curing process the white pixels seemed to be "leaking" to neighboring black pixels, limiting spatial resolution.

To test this leaking process and the effective resolution of our system, we printed vertical stripes with flakes tilted alternately to the left and right (Figure 18). We printed the stripes with different widths of 300, 250, and 200 µm. Our current setup shows good contrast at 250 µm, but reduced contrast at 200 µm. This loss in resolution could be happening for multiple reasons. First, the optics of our projector were optimized for visible light, not UV, and might be focusing imperfectly. Second, when projecting a white stripe, the chemical reaction of curing might be propagating spatially to neighboring black pixels. Finally, the flakes themselves might be causing some light scattering to neighboring pixels.

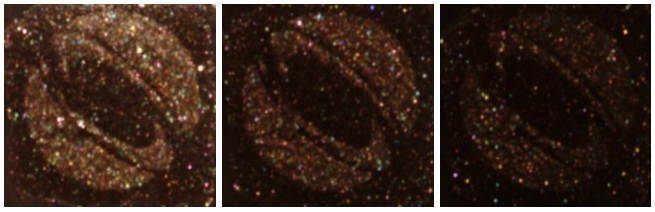

Fig. 17. SIGGRAPH logo printed with the spiral field, lit at decreasing elevation angles. The background was created with a spiral that goes all the way to vertical, yielding a dark appearance. The logo itself is specular, created with the circular field.

300 µm 250 µm 200 µm

Fig. 18. Investigating limits on resolution. Each target shows vertical stripes of two tilts, produced by the circular fields. Our system has good contrast at 300 and 250 µm, but begins to deteriorate at 200 µm.

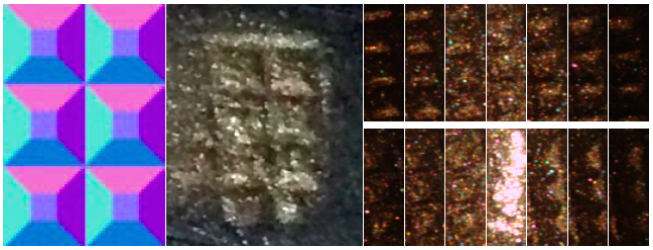

Fig. 19. Six small pyramids. *Left:* The target normal map. *Center:* Printed results under natural lighting. *Top right:* Lit from different elevation angles along the y axis (55,40,25,-20,-35,-50,-65). *Bottom right:* Lit from different elevation angles along the x axis (40,25,10,-20,-35,-50,-65).

We also printed a "bump map" with five different masks, one for each normal. Figure 19 shows them under natural lighting and also under a controlled point light.

Finally, we printed a SIGGRAPH logo with different anisotropic tangents. Figure 20 shows the sample under natural illumination as well as lit from two different azimuthal angles at constant elevation. For these samples, we used the spiral field ($\tau = 0.45$) followed by the line field for each of background and foreground.

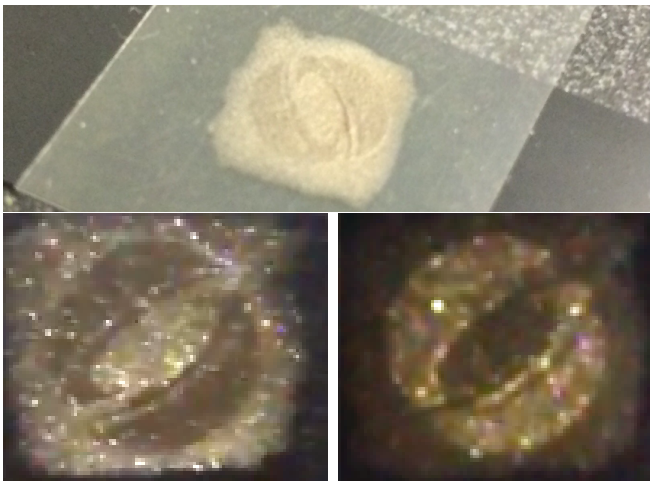

Fig. 20. SIGGRAPH logo in which foreground and background have different anisotropic tangents. This print was created in two passes, each using the spiral field to randomize the flakes' orientations, followed by the line field to achieve the desired anisotropy. *Top:* Lit under a natural environment. *Bottom:* Lit with a point light from different azimuthal angles.

8 CONCLUSION

In this work, we have shown how to use magnetic fields to control the orientation distribution of reflective flakes, resulting in surfaces exhibiting anisotropic reflectance. Our projector-based printer exposes the flakes to a time-varying magnetic field and then selectively fixes them in place with UV light. This setup was used to fabricate spatially-varying BRDFs.

We have explored several directions of variation in BRDF space that can be achieved using our technique, and characterized the limitations (due to magnetic field strength) of, for example, how specular we can make surfaces. However, there is currently no theoretical characterization of the limitations of orienting flakes with magnets, beyond simply what can be achieved with microfacet or micro-flake models. Providing such a characterization, and "gamut mapping" arbitrary BRDFs [Matusik et al. 2009; Pereira and Rusinkiewicz 2012] into the space of materials achievable with this technique is an important avenue for future work.

Another interesting direction is investigating setups that use a compact print head with magnetic control instead of a large electromagnet and projector, following the general system setup of Kokkinis et al. [2015]. This would allow for more fine-grained control over the magnetic field, in addition to permitting multiple layers of flakes, allowing for subsurface scattering phenomena.

Looking further ahead, we envision a system that combines conventional 3D printing using UV-cured resin with the ability to affect the BRDF or BSSRDF of the resulting 3D models. Even restricting ourselves to affecting an object's effective normals could allow for higher-resolution details, just as with bump-mapping in computer graphics. More generally, this type of approach would approach the ultimate goal of (one type of) appearance fabrication: being able to produce a real-world object with arbitrary shape and appearance.

ACKNOWLEDGMENTS

Thanks to Todd Zickler, Wojciech Matusik, and the members of the Princeton Graphics Lab for their helpful ideas and suggestions. This work was partially supported by NSF grants IIS-1011919 and IIS-1012147.

REFERENCES

Michael Ashikmin, Simon Premože, and Peter Shirley. 2000. A Microfacet-based BRDF Generator. In *Proc. ACM SIGGRAPH*. 65–74.

Nathalie Benninger, Claude-Alain Despland, Pierre Degott, and Edgar Müller. 2005. Method and Means for Producing a Magnetically Induced Design in a Coating Containing Magnetic Particles. Patent WO/2005/002866.

Robert L. Cook and Kenneth E. Torrance. 1982. A Reflectance Model for Computer Graphics. *ACM Trans. Graphics* 1, 1 (Jan. 1982), 7–24.

Yue Dong, Jiaping Wang, Fabio Pellacini, Xin Tong, and Baining Guo. 2010. Fabricating Spatially-Varying Subsurface Scattering. *ACM Trans. Graphics* 29, 4 (July 2010), Article 62.

Manuel Finckh, Holger Dammertz, and Hendrik P. A. Lensch. 2010. Geometry Construction from Caustic Images. In *Proc. ECCV*. 464–477.

Miloš Hašan, Martin Fuchs, Wojciech Matusik, Hanspeter Pfister, and Szymon Rusinkiewicz. 2010. Physical Reproduction of Materials with Specified Subsurface Scattering. *ACM Trans. Graphics* 29, 3 (July 2010), Article 61.

Matthias B. Hullin, Ivo Ihrke, Wolfgang Heidrich, Tim Weyrich, Gerwin Damberg, and Martin Fuchs. 2013. State of the Art in Computational Fabrication and Display of Material Appearance. In *Eurographics State of the Art Reports*. 137–153.

Wenzel Jakob, Adam Arbree, Jonathan T. Moon, Kavita Bala, and Steve Marschner. 2010. A Radiative Transfer Framework for Rendering Materials with Anisotropic Structure. *ACM Trans. Graphics* 29, 4 (July 2010), Article 53.

Takeshi Kashiwagi, Tutsuya Tamura, and Mitsuaki Narita. 1994. Painting with Magnetically Formed Pattern and Painted Product with Magnetically Formed Pattern. Patent 5364689.

Dimitri Kokkinis, Manuel Schaffner, and André R. Studart. 2015. Multimaterial magnetically assisted 3D printing of composite materials. *Nature Communications* 6 (Oct. 2015), Article 8643.

Yanxiang Lan, Yue Dong, Fabio Pellacini, and Xin Tong. 2013. Bi-scale Appearance Fabrication. *ACM Trans. Graphics* 32, 4 (July 2013), Article 145.

Anat Levin, Daniel Glasner, Ying Xiong, Frédo Durand, William Freeman, Wojciech Matusik, and Todd Zickler. 2013. Fabricating BRDFs at High Spatial Resolution Using Wave Optics. *ACM Trans. Graphics* 32, 4 (July 2013), Article 144.

Wojciech Matusik, Boris Ajdin, Jinwei Gu, Jason Lawrence, Hendrik P. A. Lensch, Fabio Pellacini, and Szymon Rusinkiewicz. 2009. Printing Spatially-Varying Reflectance. *ACM Trans. Graphics* 28, 5 (Dec. 2009), Article 128.

Marios Papas, Wojciech Jarosz, Wenzel Jakob, Szymon Rusinkiewicz, Wojciech Matusik, and Tim Weyrich. 2011. Goal-based Caustics. *Computer Graphics Forum* 30, 2 (2011), 503–511.

Marios Papas, Christian Regg, Wojciech Jarosz, Bernd Bickel, Philip Jackson, Wojciech Matusik, Steve Marschner, and Markus Gross. 2013. Fabricating Translucent Materials Using Continuous Pigment Mixtures. *ACM Trans. Graphics* 32, 4 (July 2013), Article 146.

Thiago Pereira and Szymon Rusinkiewicz. 2012. Gamut Mapping Spatially Varying Reflectance with an Improved BRDF Similarity Metric. *Computer Graphics Forum* 31, 4 (June 2012), 1557–1566.

Roger Phillips, Charlotte LeGallee, Charles Markantes, Paul Coombs, and Matthew Witzman. 2004. Methods for Producing Imaged Coated Articles by Using Magnetic Pigments. Patent 6759097.

Burt Pratt and Paul Salzberg. 1947. Process for Orienting Ferromagnetic Flakes in Paint Films. Patent 2418479.

Vladimir P. Raksha, Charles T. Markantes, Paul G. Coombs, and Dishuan Chu. 2007. Robust Multilayer Magnetic Pigments and Foils. Patent 7285336.

Vladimir P. Raksha, Charles T. Markantes, Paul G. Coombs, Roger W. Phillips, Paul T. Kohmann, Alberto Argoitia, and Neil Teitelbaum. 2009. Anisotropic Magnetic Flakes. Patent Application 20090072185.

Ludovic Thevenet. 2008. Method of Applying Makeup to a Surface by Means of a Magnetic Composition Including Reflective Particles Having Metallic Luster. Patent Application 20080127990.

Tim Weyrich, Pieter Peers, Wojciech Matusik, and Szymon Rusinkiewicz. 2009. Fabricating Microgeometry for Custom Surface Reflectance. *ACM Trans. Graphics* 28, 3 (Aug. 2009), Article 32.

Genzhi Ye, Sundeep Jolly, V. Michael Bove, Jr., Qionghai Dai, Ramesh Raskar, and Gordon Wetzstein. 2014. Toward BxDF Display using Multilayer Diffraction. *ACM Trans. Graphics* 33, 6 (Nov. 2014), Article 191.